Natural Hazards (2023) 115:2577–2601
https://doi.org/10.1007/s11069-022-05654-8

ORIGINAL PAPER

Debris flow modelling and hazard assessment for a glacier area: a case study in Barsem, Tajikistan

Kutay Yılmaz[1] · A. Ersin Dinçer[2] · Volkan Kalpakci[3] · Şevki Öztürk[4]

Received: 16 April 2022 / Accepted: 27 September 2022 / Published online: 10 October 2022

Abstract
This study analyses a previous debris flow hazard as a consequence of emerging risks related to climate and regional physical changes. In addition to the increasing flood frequencies, there is an increasing risk of mud or debris flow due to increasing temperature and heavy precipitation resulting in glacier melting. One of the most recent dramatic examples of the debris flow incident took place in Barsem, Tajikistan, in 2015. As a result of heavy precipitation and excess temperature, the melting of glaciers caused debris flow which ended up with a catastrophic damage at Barsem Town. In this study, a methodology for modelling debris flow and related hazard is developed by examining the 2015 incident in detail with a commercially available software, Hydrological Engineering Centre-River Analysis System (HEC-RAS). Simulations and hazard assessment of the incident suggest that assessment of debris flow hazard can be implemented similar to flood hazard. Moreover, it is seen that debris flow inundation area can be predicted accurately by low-resolution free-source digital elevation models (DEMs), while in the present work they could not predict the debris flow hazard assessment accurately. Sensitivity results also reveal that free-source DEMs with higher resolutions do not necessarily give better predictions than free-source DEMs with lower resolutions.

Keywords Debris flow · Soil gradation · Hazard assessment · Non-Newtonian flow · Rheological model · HEC-RAS

1 Introduction

The impact of climate change is observed all over the world. The Central Asia region is also expected to see an increase in extreme weather events in coming decades (IPCC 2018). In fact, the magnitude of the estimated warming in Central Asia is remarkably higher than

✉ A. Ersin Dinçer
ersin.dincer@agu.edu.tr

[1] Alter International Engineering and Consultancy, Ankara, Turkey

[2] Department of Civil Engineering, Hydraulics Division, Abdullah Gül University, Kayseri, Turkey

[3] GEOCE Geotechnical Consulting and Engineering, Ankara, Turkey

[4] Department of Civil Engineering, Geotechnics Division, Çankaya University, Ankara, Turkey

the global mean. More intense and longer-lasting extreme temperature events are expected in the region (Zhang and Wang 2019). According to climate trends from the beginning of the twentieth century, the reported average annual temperature increase is about 0.5–2.5 °C in the region causing the disappearance of one third of the glacial area (USAID 2018).

Different numerical techniques and various software have been used to simulate possible landslide runout or flood risk due to glacier melting. In recent years, glacier lake outburst floods (GLOFs) hazards in various regions were studied mostly with a commercially available software, Hydrological Engineering Centre-River Analysis System (HEC-RAS) (Gilany and Iqbal 2020; Zhang et al. 2021). Debris or mudflows were also investigated with HEC-RAS (Floyd et al. 2020; Gibson et al. 2021) as well as some other software like DebrisFlow Predictor (Guthrie and Befus 2021), GeoFlow_SPH (Braun et al. 2018), FLO-2D, RAMMS (Cesca and D'Agostino 2008) and r.avaflow (Mergili et al. 2017). Debris flow typically shows non-Newtonian flow behaviour with a large sediment entrainment and a high flow velocity (Jakob and Hungr 2005). Since debris and mud flows occur intermittently and after long periods of inactivity, field observations of them are nearly impossible to perform (Zimmermann and Haeberli 1992). In addition, due to the different soil and material composition, different concentration volume and complex physical interactions of particles, a generally applicable rheological model that can simulate all possible flow types is not available (Kaitna et al. 2007). Moreover, accurate detection of real topography plays an important role for debris and mud flow modelling. The accurate estimation of the amount of the soil erosion depends on the resolution of the digital elevation model (DEM). However, most studies in the literature use free-source DEMs whose best resolution are 10×10 m. Moreover, the sensitivity analysis of the resolution levels is very rare (Chidi et al. 2021). To sum up, debris and mud flows are highly case dependent and special care must be taken to simulate them correctly and to create hazard maps. To successfully predict debris and mud flow, a proper numerical model should be used, the soil properties should be well-defined, and the resolution of the DEM should be high enough.

There are studies in the literature analysing debris and mud flow. Guthrie and Befus (2021) investigated debris flow incidents in Papua New Guinea, Indonesia and Vancouver Island by a probabilistic model. A prediction code for debris flows was proposed, and the results were reasonably good for the studied cases. The model of the study was probabilistic and neglectful of some important factors such as rheology, geology, the water content in the soil. In another study, two well-known commercially available software, FLO-2D and RAMMS were used to predict debris-flow event occurred in Dolomites, Belluno, Italy (Cesca and D'Agostino 2008). Although the results were interesting, the predictions were not very close to each other since each software used different rheological models. Similarly, debris flow occurred in Hong Kong and rock avalanche in New Zealand was investigated to compare the capabilities of r.avaflow and GeoFlow-SPH codes (Tayebi et al. 2021). In the study, both codes were evaluated to be capable of estimating the run-out distance, deposition thickness, and deposition shape while maximum propagation velocities and thickness values obtained from these two different codes were remarkably different. In a recent study, debris flow hazard mitigation in Jiuzhaigou Valley, China, was performed and some control measures were proposed (Zhao et al. 2020). Moreover, Zhang et al. (2021) investigated GLOF propagation in the Poiqu River Basin, Central Himalayas. Debris flows were also observed in steep areas after wildfire which increases the susceptibility of steep slopes to debris flows. There are research analysing the post-fire debris flow runout events in various case studies (Cannon et al. 2009; Kean et al. 2019). In addition to studies focusing on the correct simulation of debris flow, risk assessment techniques for debris flow incidents were also investigated (Fuchs et al. 2007) and various vulnerability

curves as a function of flow intensity were constructed (Akbas et al. 2009; Papathoma-Köhle et al. 2012). Raetzo et al. (2002) proposed three-step procedure: identification and assessment of the hazard and risk management to generate natural hazard maps. Accordingly, hazard maps used in federal guidelines of Switzerland were constructed. Three colours, red, blue, and yellow, were used to define degrees of danger developed by using two major parameters, the intensity and the probability. Hürlimann et al. (2006) offered a methodology for debris flow hazard assessment at a local scale. Although their study focused on the catchments in Andorra, they suggested that the methodology can be applied to other mountainous areas by considering their local conditions. As can be concluded, debris flows were extensively investigated in previous studies. However, each debris flow event has unique characteristics and thus each case and related studies have a contribution to the current literature about the debris flow.

A hazardous debris flow occurred in Barsem, Tajikistan, on 16 July 2015 due to combination of high temperature, excess precipitation, rapid melting of snow, and glacier melting. Following this hazard, a technical report was published by Organization for Security and Co-operation in Europe (OSCE) investigating the assessment and distribution of debris flows in Tajikistan (Saidov and Ischuk 2018). According to the report, massive debris flows were triggered due to the increase in temperature in 2015 in the region combined with an unexpected heavy rain in the summer season. Although no human loss was reported, 56 houses were destroyed, 1100 citizens were blocked in the isolated part of the village. Main power lines supplying electricity from Pamir-1 Hydropower station were also damaged causing the electricity loss in towns around the region. According to the monitoring mission conducted by the government, there are two more glaciers that could melt (REACT 2015).

The main objective of this study is to develop a methodology for modelling debris flow and to assess hazards by considering the debris flow that occurred in 2015, Barsem, Tajikistan (referred as 2015 debris flow hereafter). For this purpose, the 2015 debris flow is studied, the total amount of glacier melting is calculated for pre-avalanche area and sediment volume loss is estimated. Using the estimated volume loss and the measured soil properties, debris flow is simulated and compared with the avalanche transit and accumulation zones. A sensitivity analysis is also performed to see the effect of DEM resolution on debris flow. In this respect, both free-source DEMs with 12.5 m and 30 m resolution as well as a DEM with 2 m resolution obtained by field survey are used and results are compared. In addition, hazard classifications defined for Newtonian flows and non-Newtonian debris flows are compared and the results suggest that hazard classifications derived for Newtonian flows are as successful as the ones derived for debris flow, for the investigated problem.

2 Study area

The study area is located in the town of Barsem, downstream of Pamir Mountains, between 37°–38° North Latitudes and 71°–72° East Longitudes, in a region close to the Afghanistan border of Tajikistan. The area is surrounded by mountains and valleys, which makes the region vulnerable to floods, mudflow and debris flow. Moreover, glaciers exist above 4200 m above the sea level (asl). As a result of climate change, lakes have been formed due to the melting of glaciers around the region. The study area covers the extended area that the 2015 debris flow incident took place. The location and the view of study area as well as

photographs of the accumulation area and the valley near Barsem Town are given in Fig. 1. Catchment area and glaciers are shown with green and white, respectively. Besides, debris accumulation and landslide areas are also illustrated with the red and black line, respectively. Landslide area is defined according to the previous report about the incident (Fuchs 2015) and field surveys.

3 Methodology

Various data are needed to successfully simulate a debris flow. Accordingly, total volume of the 2015 debris flow incident is calculated. Then, soil properties are determined using the samples taken from the flow channel and the transported sediment. The appropriate non-Newtonian model is chosen after defining the soil gradation. By including the hourly precipitation data and the surface roughness, the hydraulic model is implemented. After achieving the convergence, the hydraulic model is used to simulate the 2015 debris flow incident. The detailed description of the workflow of the

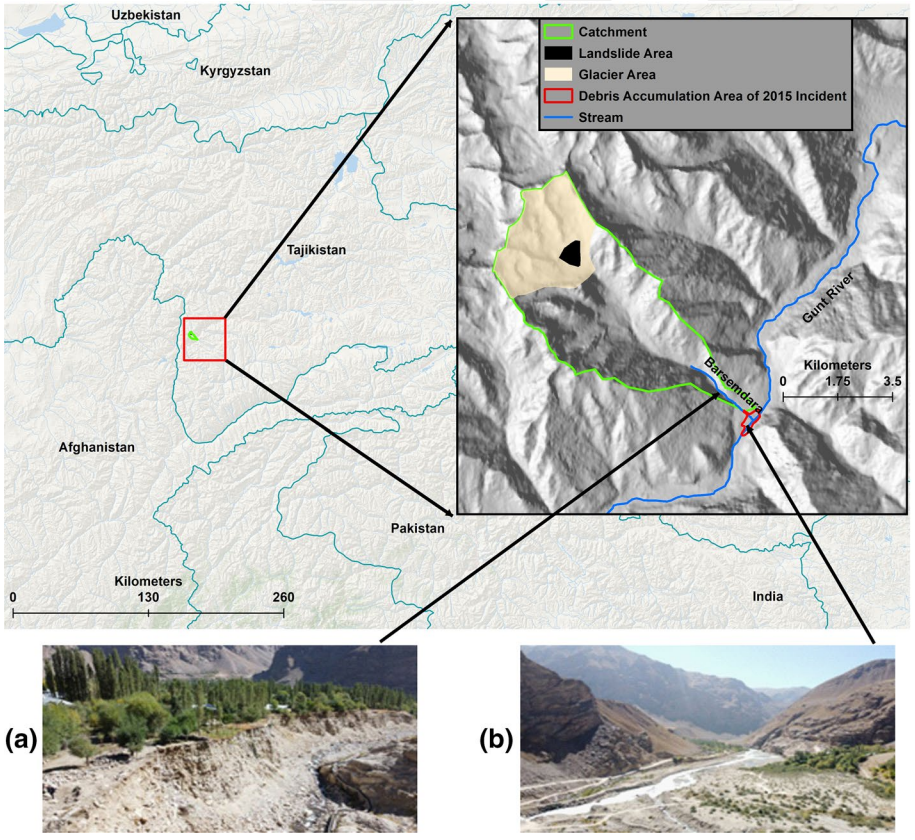

Fig. 1 Satellite view of the study area and photographs of **a** the valley near the Barsem Town and **b** the accumulation area of catchment

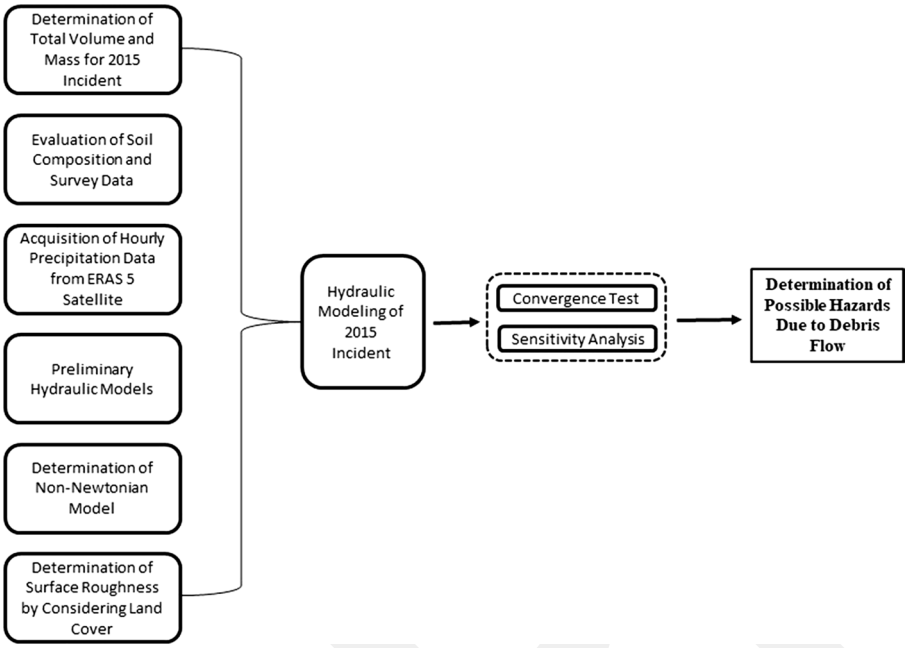

Fig. 2 Workflow of the study

study is presented in Fig. 2. The following sections contain a detailed description of each effort that is made to simulate the 2015 debris flow incident.

3.1 Soil properties

Sieve analyses are performed on the samples taken from the flow channel (FC), the transported sediment (TS) and their locations are given in Table 1 and Fig. 3. The results show that the samples collected from different parts of the area have reasonably similar characteristics. The resulting values are summarized in Table 1 and the corresponding average particle size distribution curve is given in Fig. 4. Sieve analyses results suggest that the soil at site is such a coarse material that only 1.4% of the total mass is of fine particles while the rest is fully composed of coarse particles. Based on the presented test results, the soil is classified as "GW: Well-graded Gravel" (ASTM 2017) with an approximate gravel content of 68% in the soil mass.

The samples taken from the borrow pits along the region are also tested in the laboratory to determine their basic physical properties like density (ρ), specific gravity (γ), natural and maximum water content (W_n and W_{max}, respectively), void ratio (e), porosity (n) and degree of saturation (Sr). The borrow pit locations are shown in Fig. 3, and the results are summarized in Table 2. According to Table 2, the transported sediment has average properties of $W_n = 2.24\%$ (1.80–2.70%), $\gamma = 2.70$ g/cm^3, $\rho_{bulk} = 2.19$ g/cm^3 (2.11–2.23 g/cm^3), $\rho_{dry} = 2.14$ g/cm^3 (2.05–2.19 g/cm^3), $e = 0.26$ (0.23–0.31), $n = 0.21$ (0.19–0.24), $W_{max} = 9.68\%$ (8.70–11.50%) and Sr = 23.19% (17.60–27.90%).

Table 1 Sieve analysis test results

#	Sample	Location	Sieve Size (mm) (% Passing)											
			200	70	40	20	10	5	2.5	1.25	0.63	0.31	0.15	0.075
1	ш-1	TS	100	82.2	75.5	59.7	47.9	44	41.1	34.8	22.3	12	4.9	2.7
2	ш-3	TS	91	79.7	74.7	72.3	55	50.7	48.5	41.4	19.9	5.1	0.9	0.4
3	ш-4	FC	92	77.2	69.5	61.1	41.8	36.2	33.9	27.7	15.4	5.6	1.3	0.7
4	ш-5a	TS	100	91.5	76.4	56.6	46	38.6	32.7	29.2	12.2	1	0.2	0.1
5	ш-5b	TS	87	70.8	59.7	58.9	33.6	30.4	27.5	19.5	4.8	1.3	0.4	0.2
6	ш-6a	TS	100	83.8	71.5	56.6	41.5	30.7	28	19.3	7.3	2.5	1.1	0.5
7	ш-6b	TS	90	80.6	73.1	66.9	44.5	33.2	30.2	26.6	19.4	14	9.2	5.1
8	ш-7a	TS	100	80.3	73.1	62.7	34.9	27.7	23.2	20.7	13.7	8.4	5	2.9
9	ш-7b	TS	90	73.2	63.6	52.3	29.2	23.9	21	18.1	9	3.6	1.4	0.9
10	ш-8	TS	90	79.7	74	70.4	54.3	51	48.4	45.5	33.9	23.1	6.2	3
11	ш-9	TS	88	71.2	63.4	60.5	40.4	33.6	29.4	18.8	6.3	1.7	0.5	0.2
12	ш-10	FC	94	86.2	71.2	59.7	37.2	32.9	29.4	25.1	14	6.9	2.9	0.8
13	ш-11	FC	91	77.3	65.5	59.5	44.3	39.3	35.7	28.2	13.9	5.7	1.7	0.8
Average			93.3	79.5	70.1	61.3	42.4	36.3	33	27.3	14.8	7	2.7	1.4

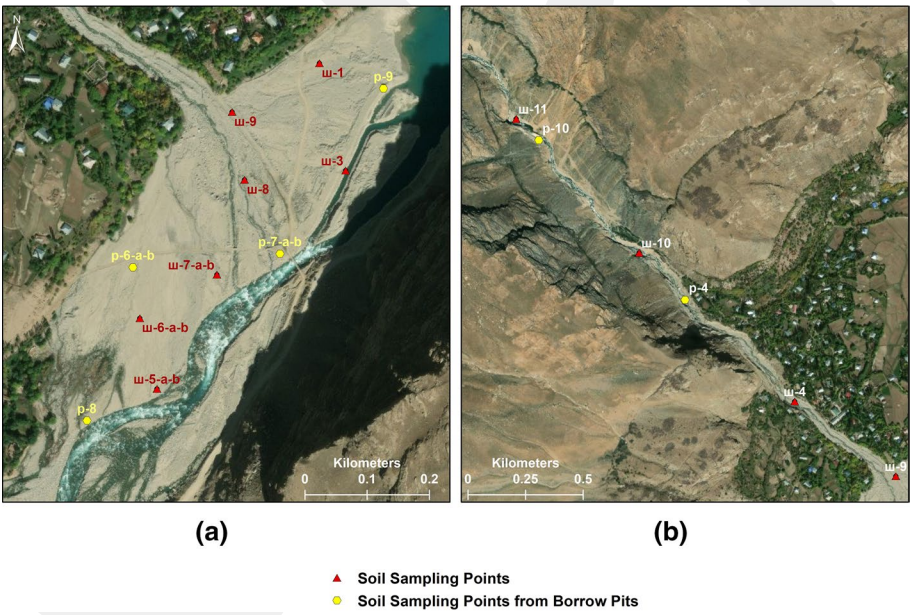

Fig. 3 Soil sampling points **a** in the debris accumulation area and **b** at the valley

3.2 Digital elevation model (DEM)

In order to implement the hydraulic model, the DEM produced before the 2015 incident is obtained from the local authorities of Tajikistan with a 2 m resolution. To produce the DEM after the incident, field studies are performed. With the help of topographic and

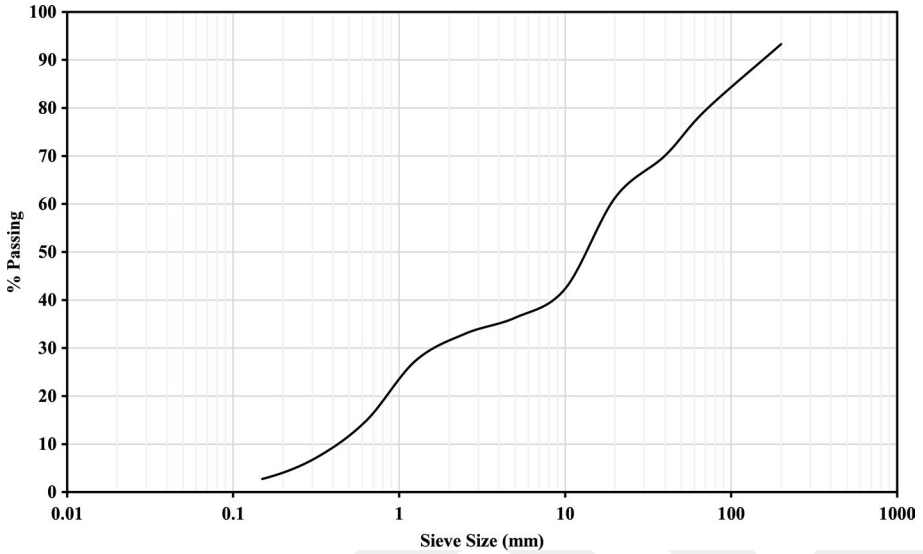

Fig. 4 Average particle size distribution curve

planimetric field data, elevation models and contours of areas are passed through edit stations, and the DEMs are generated, including the arrangement of land features and consistency. The work area is approximately 250 km^2 and the data are processed in the seasons between May and September to minimize the snow cover. Field works take about one week and 4 DEMs are obtained. For hydraulic modelling, the DEMs are merged to obtain a single DEM. The corresponding DEM of the study area as well as the elevation difference between the DEMs generated before and after the 2015 debris flow incident is shown in Fig. 5. Instead of presenting DEMs before and after the incident in full scale, showing the elevation difference is preferred. Because the elevation difference is mainly observed around the landslide and glacier area and the mean thickness of the sliding land is about 3 m. Therefore, the difference between the two DEMs is small and cannot be clearly captured.

Vertical accuracies of the DEMs are generally dependent on slope. In steeper terrain, the same level of vertical accuracy cannot be guaranteed as for flat or moderately undulated terrain. In the study, the relative vertical accuracy is higher than 2 m (LE90) on slopes less than 20% and higher than 4 m (LE90) on slopes higher than 20%. Besides, the absolute horizontal accuracy is higher than 6 m with a circular error of 90% (CE90). To avoid possible deviations from the real physical situations, possible covers, shadows, etc. are extracted from the DEM. The resolution of the DEM is 2 m, and the DEM is delivered in geographic projection with Universal Transverse Mercator (UTM) coordinate system WGS84 horizontal datum in Zone 42 and EGM96 geoid.

In addition to the DEM of 2 m resolution that is obtained from the field study, free-source DEMs are considered in order to examine the effect of the DEM resolution on debris inundation. For this reason, the DEM with 12.5 m resolution is obtained from ALOS PALSAR which provides radiometric terrain corrected elevation data. The lower resolution DEM of 30 m is obtained from the SRTM which provides elevation data of Space Shuttle Endeavour. The ALOS data are formed by the data for the year of

Table 2 Laboratory test results

#	Pit	Location	Wn (%)	γ (g/cm^3)	ρ_{bulk} (g/cm^3)	ρ_{dry} (g/cm^3)	e	n	Wmax (%)	Sr (%)
1	p-4	FC	2.00	2.70	2.11	2.07	0.31	0.24	11.40	17.60
2	p-6	TS	2.70	2.69	2.11	2.05	0.31	0.24	11.50	23.40
3	p-6	TS	1.90	2.70	2.23	2.19	0.23	0.19	8.70	21.90
4	p-7	TS	2.20	2.70	2.22	2.17	0.24	0.20	9.00	24.50
5	p-7	TS	2.60	2.70	2.21	2.16	0.25	0.20	9.30	27.90
6	p-8	TS	2.70	2.70	2.20	2.14	0.26	0.21	9.70	27.70
7	p-9	TS	2.00	2.70	2.21	2.17	0.24	0.20	9.00	22.10
8	p-10	FC	1.80	2.70	2.22	2.18	0.24	0.19	8.80	20.40
Average			2.24	2.70	2.19	2.14	0.26	0.21	9.68	23.19

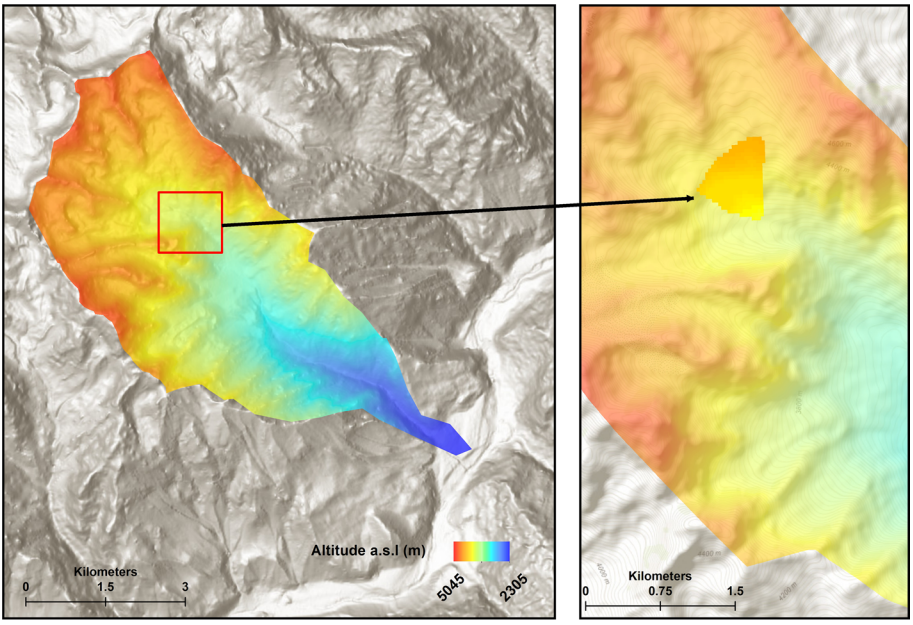

Fig. 5 DEM of the study area **a** before 2015 debris flow incident and **b** the elevation difference between DEMs taken before and after the incident

2011 whereas SRTM source covers the data for the year of 2013. In the DEMs, there are slight differences especially for the areas above 4200 m due to the formation of glaciers. Since these differences would have slight effect on the inundation area, only the resolution of the DEMs is taken as the main variable for the sake of sensitivity analysis. The DEM obtained from the field works is used throughout the manuscript. In sensitivity part, all three DEMs are used.

3.3 Hydraulic modelling

Hydraulic modelling is implemented by using HEC-RAS. Two-dimensional hydraulic modelling approach is considered. Physical behaviour of fluids is mathematically expressed by Navier–Stokes equations and the appropriate turbulence model. If the vertical disturbances are relatively small compared to the longitudinal ones, the shallow water equations are considered to represent the fluid flow. Therefore, two-dimensional modelling of the study area suggests solving the shallow water equations. The shallow water equations are simplified form of Navier–Stokes equations. The theoretical background of the equations that are used in the solver can be found in the study of Brunner (2021). Additionally, a detailed information about the rheological models and the related equations can be found in the study of Gibson and Sanchez (2020).

3.3.1 Sediment volume and scour calculations

Two DEMs are obtained illustrating before and after the 2015 debris flow incident as shown in Fig. 5. To calculate the amount of landslide that conveyed through the catchment, geographic information system (GIS) works are implemented so that the difference between two DEMs above 4200 m asl given in Fig. 5b can be obtained. By taking surface integral of the DEM obtained by subtracting two DEMs results in 904,897 m^3 of volume which is the debris conveyed through the catchment. According to Fuchs (2015) Dokukin et al. (2019) and REACT (2015), the 2015 incident took place between 16 and 20th of July and approximately 1.5 million m^3 of debris was transported throughout the incident. They estimated the debris volume from the field observations, and it was mentioned that roughly 1 million m^3 of the volume originated from the landslide occurred above 4200 m asl. Therefore, the volume calculation methodology of differentiating two different DEMs and integration of the difference ended up with similar results compared to the field study.

Cross sections of the DEMs taken before and after the 2015 debris flow incident are compared and the amount of scouring is calculated. To show the differences in the cross sections, three points are chosen and the locations of them are shown in Fig. 6. The cross sections are also validated with in situ measurements. The comparison of cross sections is also given in the same figure. The scour in the channel can be seen clearly. The total amount of scour is calculated from the difference in bed elevations throughout the catchment area of the DEMs before and after 2015 debris flow incident and found to be approximately 550,000 m^3. Consequently, by adding the volume of the landslide and the scour, a

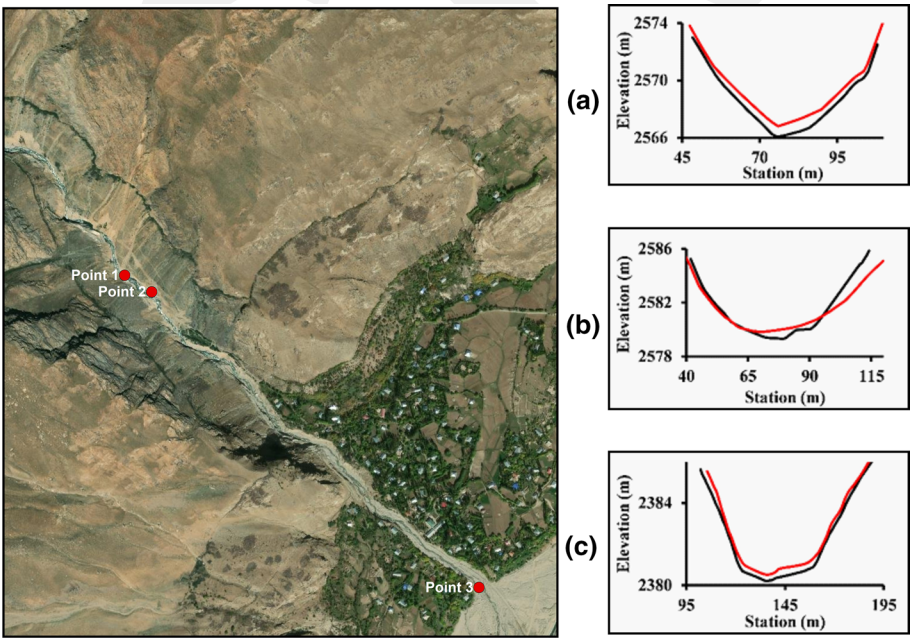

Fig. 6 The comparison points and related cross sections taken from the DEM before (red continuous line) and after (black continuous line) the 2015 debris flow incident from top to bottom **a** Point 1, **b** Point 2 and **c** Point 3

total volume of approximately 1,455,000 m^3 soil is transported which is consistent with the previously published report (Fuchs 2015).

3.3.2 Rheological model and flow classification

Field measurements show that solid concentration of the flow is very high. Flows having high solid concentration can be classified as mud floods, mudflows and debris flows. In general, turbulent shear stress is dominant in mud floods whereas yield and viscous stresses are dominant in mudflows. In debris flows, dispersive stress is dominant (O'Brien and Julien 1988). Mud floods consist of non-cohesive particles and show fluid behaviour. The sediment concentration of the mixture is 40% at most. Mudflows usually include silts and clays, so they behave like a highly viscous fluid flow. The volumetric sediment concentration of mudflows ranges from 45 to 55% (O'Brien and Julien 1988). Debris flows can be classified as the mixture of boulders and woody debris. According to the landslide classification system based on the study of Varnes (1978), "debris" is defined as "contains a significant proportion of coarse material; 20% to 80% of the particles are larger than 2 mm, and the remainder is less than 2 mm". As is seen in Fig. 4, 68% of the mobilized mass is larger than 2 mm while the rest is smaller than 2 mm. Therefore, the mobilized mass can be classified as "debris".

For an approximate amount of 1.5×10^6 m^3 of soil:

$$n = \frac{V_{\text{void}}}{V_{\text{soil}}} = \frac{V_{\text{void}}}{1.5x10^6} = 0.21 \Longrightarrow V_{\text{void}} = 315000\,\text{m}^3 \tag{1}$$

$$S_r = \frac{V_{\text{water}}}{V_{\text{void}}} = \frac{V_{\text{water}}}{315000} = 0.232 \Longrightarrow V_{\text{water}} = 73000\,\text{m}^3 \tag{2}$$

$$V_{\text{solid}} = V_{\text{soil}} - V_{\text{void}} = 1500000 - 315000 = 1185000\,\text{m}^3 \tag{3}$$

$$V_{\text{air}} = V_{\text{void}} - V_{\text{water}} = 315000 - 73000 = 242000\,\text{m}^3 \tag{4}$$

where V_{void}, V_{soil}, V_{solid}, V_{water} and V_{air} are volume of voids, soil, solid, water and air, respectively.

Based on the laboratory tests and Eqs. (1–4), 1.185×10^6 m^3 of the total mobilized volume is estimated to be composed of solid particles while the rest is void. Additionally, 73,000 m^3 of void is estimated to be filled with water at natural state. From the precipitation data taken from ERAS-5 satellite shown in Fig. 7, which provides hourly estimates of climate variables between 16 and 20 July 2015, total precipitation amount is calculated as 943,000 m^3 for 2015 Barsem flow area.

Since it is very hard to estimate the water content of the mobilized mass just prior to the mobilization, the volumetric concentration (C_v) of the mobilized mass is calculated based on two extreme cases to determine the possible range of the volumetric concentration. In case 1, it is assumed that the soil is at its natural water content. Firstly, the soil gets fully saturated by the precipitation and the mass is mobilized with the remaining part of the precipitation. In case 2; the soil is assumed to get fully saturated prior to the precipitation due to the melting of glaciers and the precipitation is fully participated in the flow.

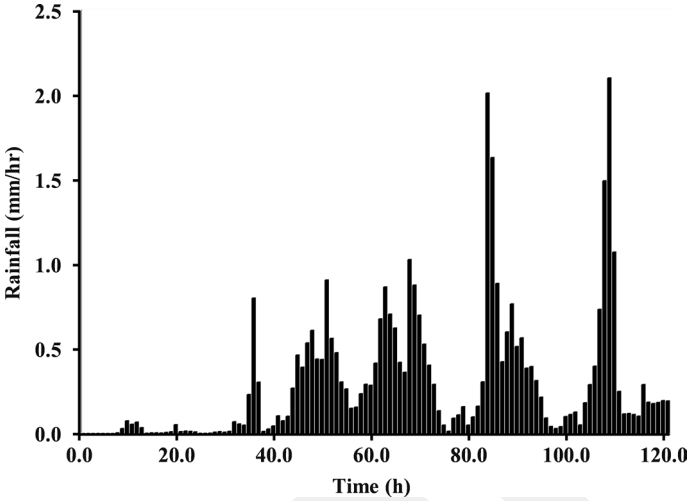

Fig. 7 ERAS-5 Precipitation data

$$\text{Case-1}: C_v = \frac{V_{\text{solid}}}{V_{\text{solid}} + V_{\text{water}}} = \frac{1185000}{1185000 + 943000 - 242000} \cong 63\% \tag{5}$$

$$\text{Case-2}: C_v = \frac{V_{\text{solid}}}{V_{\text{solid}} + V_{\text{water}}} = \frac{1185000}{1185000 + 943000} \cong 56\% \tag{6}$$

Equations (5) and (6) suggest that the volumetric concentration of the mobilized flow ranges within a narrow band of C_v = 56–63% with an approximate average of 60%. The soil sample is shown with red polygons in Figs. 8 and 9. According to Fig. 8, the flow can be classified as a non-Newtonian debris flow (Davies 1990). Furthermore, regarding the adapted classification of the debris flow given in Fig. 9 (Coussot and Proust 1996), the flow is granular debris flow. Therefore, the granular debris flow model and Mohr–Coulomb equations are used in this study.

Considering the elevation differences between the start and the end point of the debris flow and horizontal distances, the bulk internal friction angle of the flow material is calculated as $\varphi_b = 12.8°$.

3.3.3 Hydraulic model implementation

Boundary conditions are determined for the 2015 debris flow incident by considering the soil composition, field survey data and precipitation data. The ERAS-5 satellite image is used to obtain multidimensional raster for determining the precipitation data. Spatially varied surface roughness is calculated by considering land cover of the region. For this purpose, land cover of the study area is obtained from the CORINE satellite images in a raster format. Land cover of the study area for the year 2012 and the year 2018 are determined and presented in Fig. 10. The average roughness coefficients are also given in Table 3. A slight difference in the land cover is observed. This difference is ignorable.

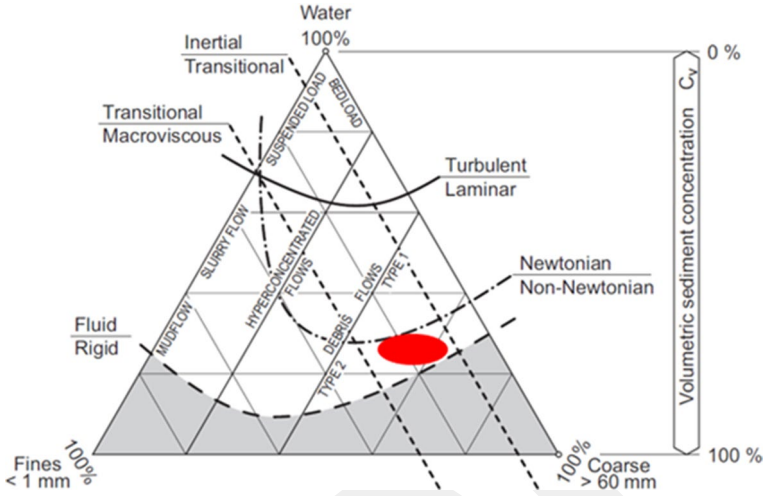

Fig. 8 Flow characteristics and classification of the debris flows (Davies 1990) (red polygon shows the soil sample in this study)

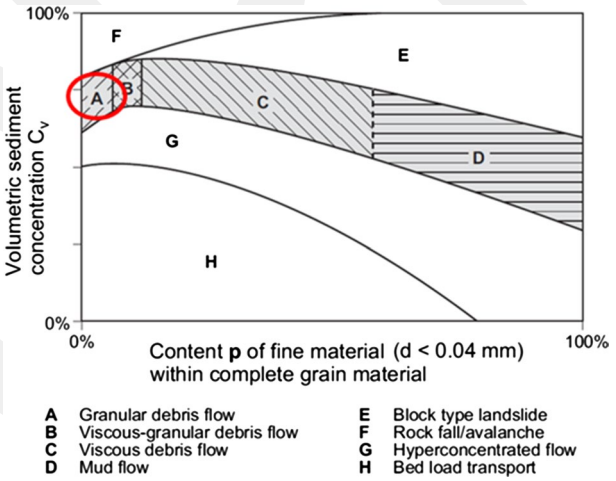

Fig. 9 Adapted classification of the debris flows and other mass movements induced by gravity (Coussot and Meunier 1996) (red polygon shows the soil sample in this study)

3.3.4 Initial configuration of the model and the convergence test

A hydrograph should be derived to simulate any GLOF. In the hydrograph peak discharge, Q_p, and breaching time, T_p, are the two important parameters. Empirical equations to find the peak discharge and breaching time are proposed in the absence of measured data (Froehlich 1995; Wahl 2004).

$$Q_p = 0.607V^{0.295}h_w^{1.24} \tag{7}$$

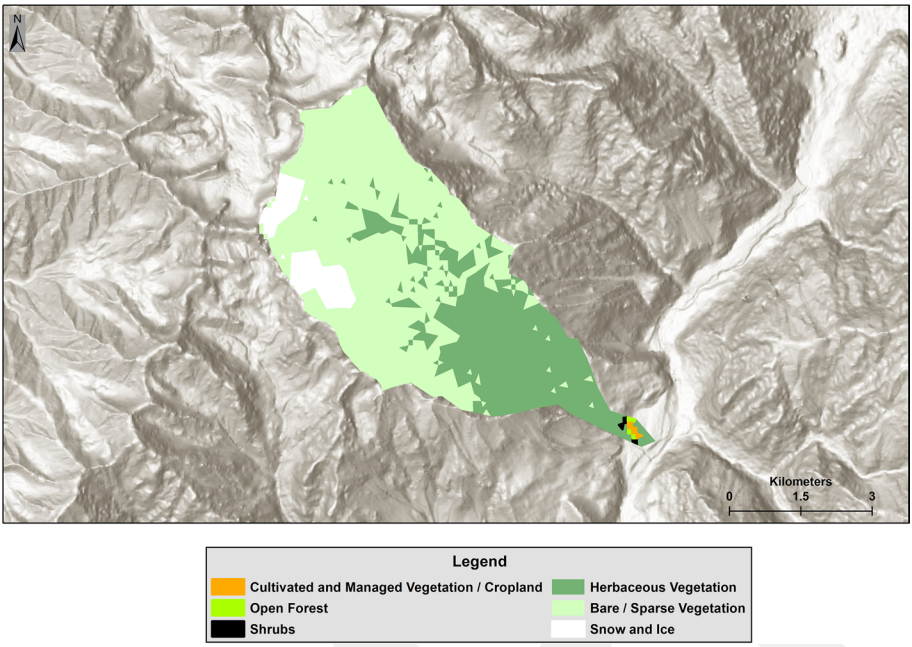

Fig. 10 Spatially varied land cover of the study area obtained from the CORINE satellite images for WGS 1964 UTM Zone 42 N

Table 3 Average roughness coefficient based on CORINE

Cover	Roughness
Shrubs	0.050
Herbaceous vegetation	0.035
Cultivated and managed vegetation/cropland	0.040
Bare/Sparse vegetation	0.027
Snow and ice	0.010

$$T_p = 0.00254V^{0.53}h_b^{-0.9} \tag{8}$$

where h_w is the depth of water above breach invert at time of failure, h_b is the height of breach and V is the outburst volume which can be calculated from empirical equations (Cook and Quincey 2015),

$$V = 60A - 6281700 \tag{9}$$

where A is the area. The applications and validations of the aforementioned equations are presented in the previous studies (Wahl 2004; Zhang et al. 2021). When those equations are applied to the 2015 Barsem debris flow incident, a peak discharge and breaching time of approximately 7000 m^3/s and 30 min are calculated, respectively. According to the report of the 2015 debris flow incident, at least 14 major debris flows occurred between 16 and 20th July 2015 (Fuchs 2015). Therefore, the debris flow incident took about 5 days. In order to include the effect of 14 different debris flows on the hydrograph, single

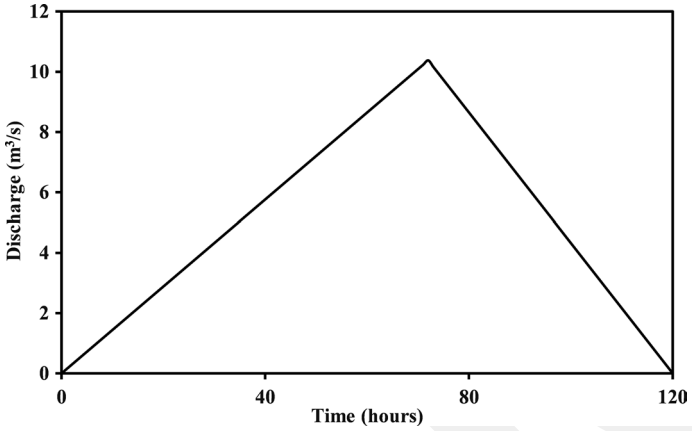

Fig. 11 Breach hydrograph

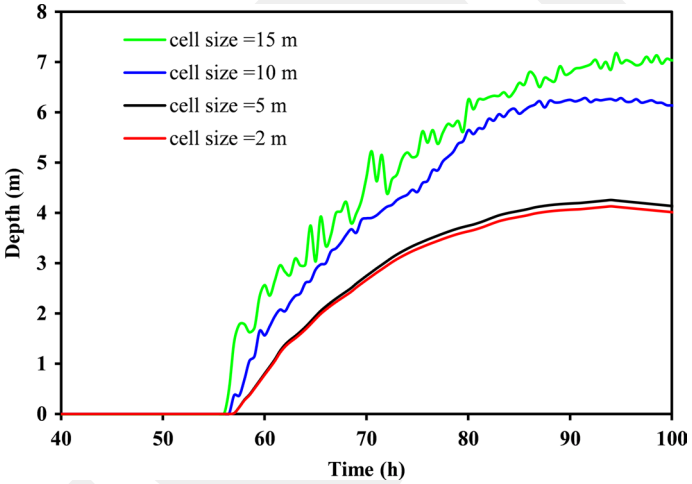

Fig. 12 Convergence test

hydrograph is generated instead of using different hydrographs for each debris flows. A hydrograph, shown in Fig. 11, is generated with the known total sediment volume and the precipitation amount (generated from ERAS-5 satellite). Since the peak discharge is lower and breaching time is higher than the ones calculated from empirical equations, slower debris flow is expected. However, simulated inundation areas and hazard assessments, taking both the depth and velocity of the flow into account, are similar to the results of the incident. Therefore, it can be deduced that the hydrograph can reflect 14 different debris flows satisfactorily.

Simulation results of the hydraulic model are compared with the inundation area of the 2015 debris flow incident. The hydraulic model with a DEM, resolution of 2 m, of the 2015 incident is constructed after determining the cell size. To determine the cell size, a convergence test is conducted for the depth at point 3 whose location is given in Fig. 6. Convergence test results, presented in Fig. 12, suggest that the mesh independency is

satisfied when the cell size is approximately 5 m. It should be noted that the final debris depth shown in Fig. 13 is different from the scour depth in Fig. 6. The reason is the date when the DEM after the incident is generated. The simulation lasts about 5 days. However, the DEM is generated 6 years after the 2015 debris flow incident. Therefore, the accumulated sediment has moved to downstream as a result of environmental factors and human activity.

3.4 Hazard assessment

Hazard assessment is often implemented by considering flow depth and velocity. Although certain values of flow depth or velocity pose danger, relating both parameters and determining thresholds is sometimes a more convenient way of defining the hazard. For this reason, several methods are proposed to assess hazard both for Newtonian and non-Newtonian fluids. Assessment of hazard depends on forces that may be applied by fluid to structures or vehicles as well as human. Therefore, the forces that may be exerted by Newtonian and non-Newtonian fluid of the same depth and velocity would not be the same due to different densities. The density of the debris flow would be higher compared to a Newtonian fluid. Therefore, exerted force at the point of consideration should be higher than the force by water. For this reason, several techniques

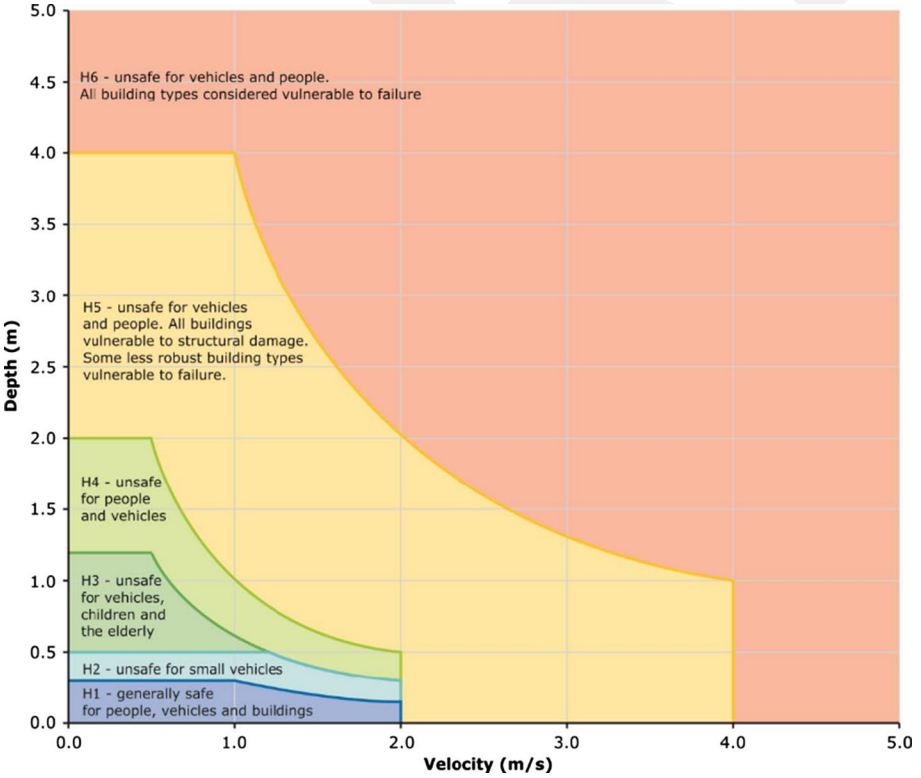

Fig. 13 Flow hazard curves (Smith et al. 2014)

were developed to assess hazard that may be caused by non-Newtonian fluids (Fuchs et al. 2007; Akbas et al. 2009, and Papathoma et al. 2012).

According to a widely used and accepted Newtonian hazard classification (Smith et al. 2014), hazard curves shown in Fig. 13 are defined.

By considering concept of risk and vulnerability, Fuchs et al. (2007) derived a quantitative debris flow vulnerability function.

$$y = 0.11x^2 - 0.02x \tag{10}$$

where x is the debris flow intensity and y is the vulnerability. According to vulnerability function "0" means that the structure is safe, while "1" means that it is mostly vulnerable.

A similar study was conducted to define an empirical vulnerability function for debris flows by Akbas et al. (2009).

$$y = 0.17x^2 - 0.03x \tag{11}$$

Papathoma-Köhle et al. (2012) presented a methodology for the development of a vulnerability curve. The vulnerability curve is a function of intensity similar to the studies of Fuchs et al. (2007) and Akbas et al. (2009).

$$y = 1 - e^{-0.27\left(\frac{x+1.287}{1.287}-1\right)^{2.974}} \tag{12}$$

4 Results

The inundation area of the 2015 debris flow incident is the most important data for the validation process. In fact, apart from the total amount of sediment relocated, the inundation area is the only data for the validation. The spatially varied depth, velocity, and hazard map derived for Newtonian fluids (Smith et al. 2014) as well as the inundation area obtained from simulation results of HEC-RAS are shown in Fig. 14. In addition, the debris area obtained from the satellite view regarding before and after the 2015 debris flow incident is presented in Fig. 15 in which both the hazard classifications developed for Newtonian (Smith et al. 2014) and debris flow (Fuchs et al. 2007) are shown. As can be understood from the figures, the hydraulic model works reasonably well in terms of determining the inundation area. The depth of debris at the river is found to be approximately 22 m, while it is about 4 m at the just upstream of the accumulation area. The velocity of debris flow is low. This is due to the high duration of the event resulting in low discharges, which is shown in Fig. 11. In the simulation results, debris flow hazard assessment is implemented by considering the study of Fuchs et al. (2007) and Smith et al. (2014). In this study, the fluid is the debris which has different physical behaviour compared to a Newtonian fluid. Therefore, it is expected to obtain higher hazard by the debris if the velocity and the depth of the flow were assumed to be the same with water. Nevertheless, calibration results of Newtonian hazard classification suggest that debris inundation area is prone to H5 and H6 hazard class which is compatible with the 2015 debris flow incident. What is more, it is seen that both Newtonian and debris flow hazard assessments give similar results and they both predict the inundation area satisfactorily.

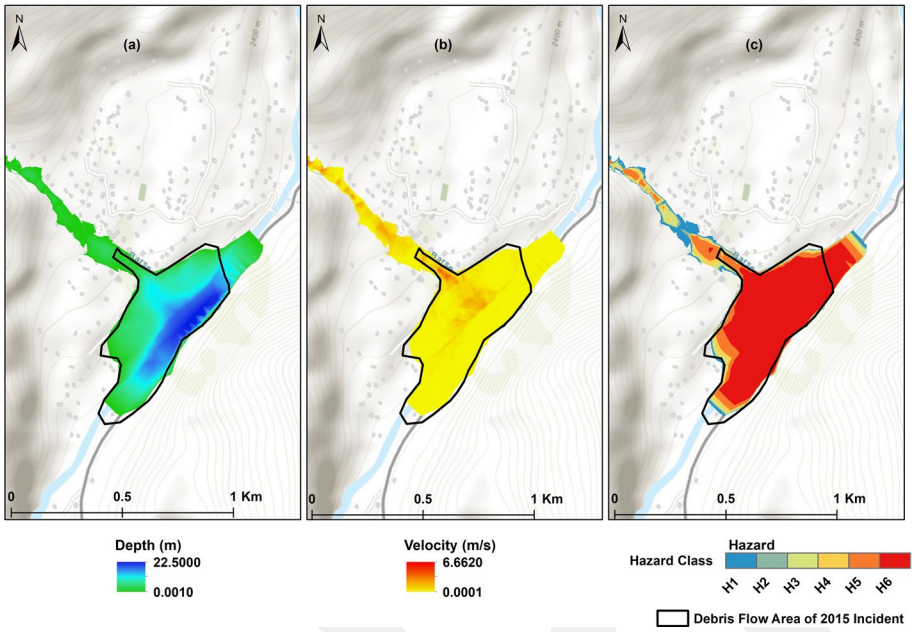

Fig. 14 Model results of **a** depth, **b** velocity and **c** hazard class

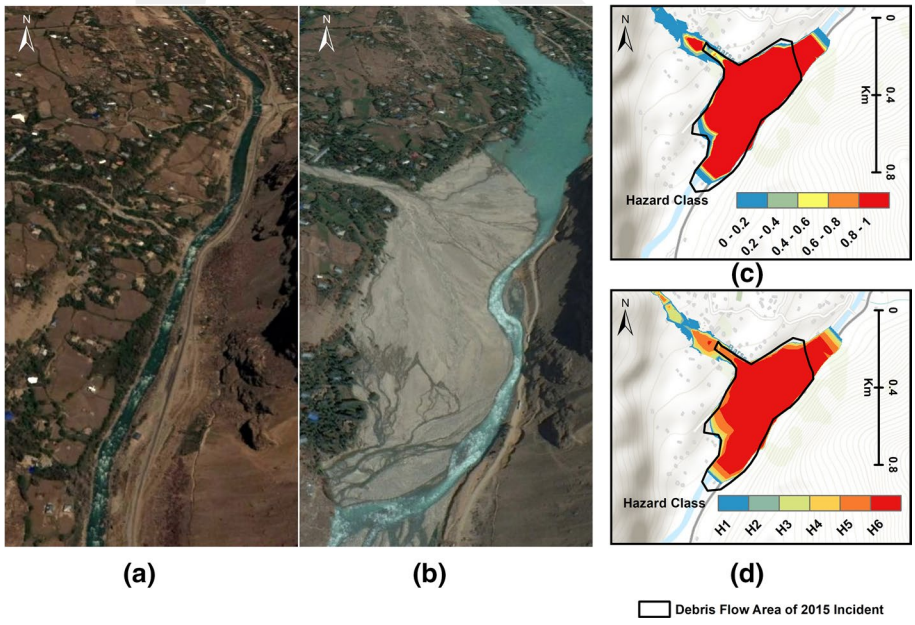

Fig. 15 Satellite views of the study area **a** before and **b** after the debris flow incident and hazard classes calculated from **c** Fuchs et al. (2007) and **d** Smith et al. (2014)

5 Discussion of results

5.1 Sensitivity analysis

A sensitivity analysis is carried out by considering three different DEMs with a resolution of 2 m, 12.5 m and 30 m obtained from the field, Advanced Land Observing Satellite (ALOS) and the Shuttle Radar Topography Mission (SRTM) of NASA, respectively.

Throughout the process, all the numerical parameters such as mesh size, time step size and boundary conditions are kept as the same to investigate the effect of DEM resolution on debris inundation. The resulting inundation area of the 2015 debris flow incident for different DEMs having various resolutions are given in Fig. 16. As can be realized from the figure, the DEM with 2 m resolution predict the inundation area more accurately as expected. Although there are slight differences, other DEMs could also predict the inundation area satisfactorily. The total inundation area is calculated as approximately 0.31, 0.35 and 0.32 km^2 for 2 m (LIDAR), 12.5 m (ALOS) and 30 m (SRTM) resolution of DEMs, respectively. At the upstream of the inundation area, there are scattered debris, which can be assumed as computational error with discontinuity due to the relatively low resolution of ALOS and SRTM DEMs.

The debris flow depth history at point 3, presented in Fig. 6, is given in Fig. 17. Although the simulated inundation areas are similar, there are considerable differences in debris flow depth observed at point 3. Additionally, the time when the debris reaches to point 3 is different. If results of the 2 m resolution DEM are assumed to be the best, the SRTM DEM predicts the maximum depth of debris flow better than the ALOS DEM. The reaching time of the SRTM DEM is also closer to the one obtained from the 2 m resolution

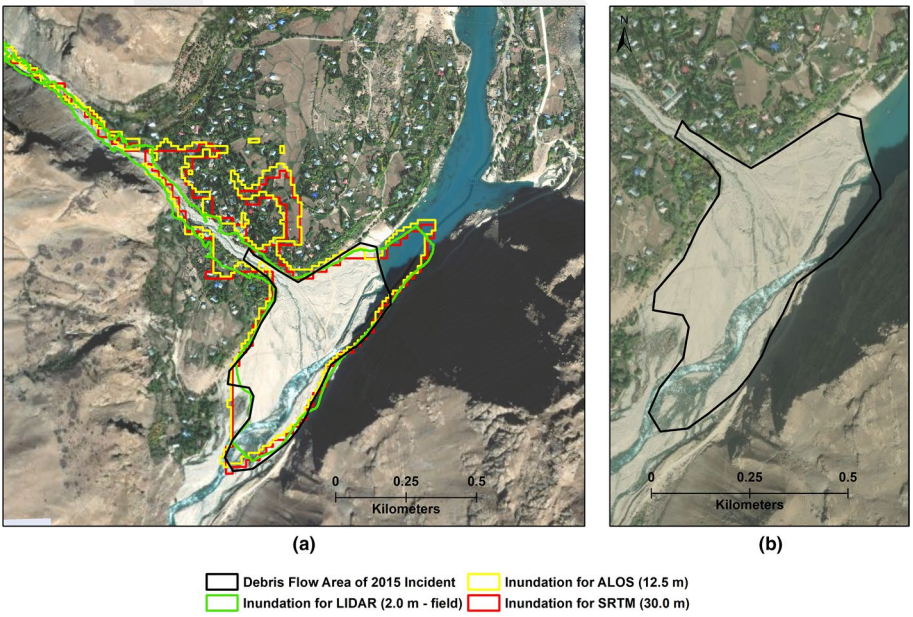

Fig. 16 **a** The resulting inundation area of the 2015 debris flow incident for the DEMs taken from different sources and **b** representation of the inundation area obtained from the field

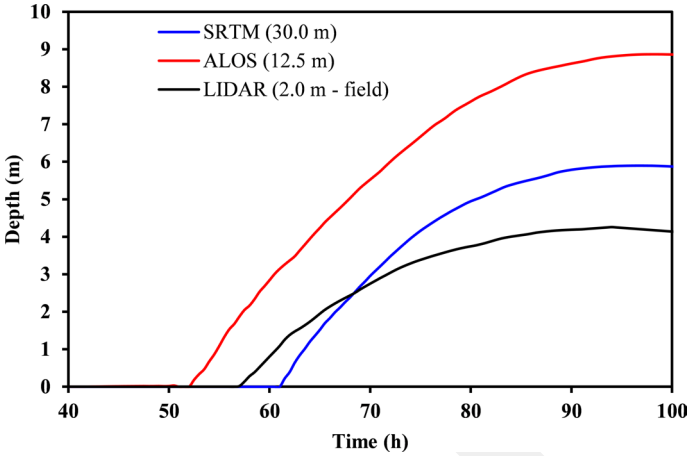

Fig. 17 The debris flow depth history of point 3

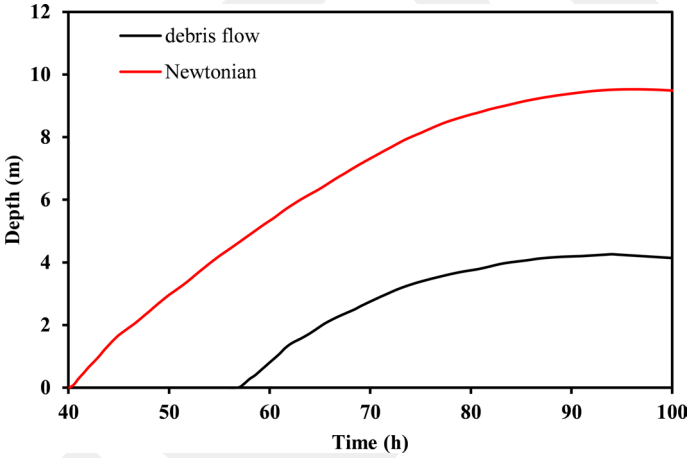

Fig. 18 Time history of debris and Newtonian flow

DEM. The results reveal that although the resolution of the ALOS DEM is higher, the SRTM DEM gives better predictions for the hazard area investigated in the present study.

5.2 Hazard duration and comparison of Newtonian and non-Newtonian flows

The arrival of the debris to point 3 takes about 60 h as shown in Fig. 17. This is mainly due to the hydrograph. The hydrograph is generated by considering 14 different debris flows observed in five days. By keeping the total sediment volume the same with the measured volume, the peak discharge is decreased to satisfy the total debris flow duration. Since the discharge is small, slow accumulations throughout the catchments are observed. To understand the differences between Newtonian and debris flow, simulations are repeated

by using the same hydrograph for Newtonian fluid. Time history of debris and Newtonian flows is given in Fig. 18. Newtonian fluid reaches point 3 approximately 20 h earlier than the debris flow which is consistent with the theory. The final depth of debris flow is approximately one-third of the final depth of Newtonian fluid. However, the accumulation of Newtonian fluid is not expected to be as devastating as debris flow due to the density difference. Although the incident took place in 2015, the sediment due to debris flow is still in the area.

5.3 Comparison of different hazard assessment techniques

Hazard caused by Newtonian fluids such as water is often assessed by considering flow depth and velocity. Widely used and accepted method of assessing Newtonian fluid hazard was proposed by Smith et al. (2014) by dividing hazard into six classes. On the other hand, risk assessment for non-Newtonian fluids is often implemented by considering the flow depth. As shown in the previous part, the hazard assessment method for Newtonian fluids provides useful results in terms of hazard classes for the case of debris flow. In this part, several debris flow risk assessment techniques are compared with each other and the assessment method of Newtonian fluid hazard. The comparison of four methods is presented in Fig. 19. Although equations for determining the vulnerability is different, three different methods suggest nearly the same results. It should be noted that all three studies about debris flow risk assessment are limited with the flow depth of 2.5 m which is exceeded in the inundation area of the present study. In addition, the hazard classification proposed for Newtonian fluids is also similar with the techniques proposed for debris flow

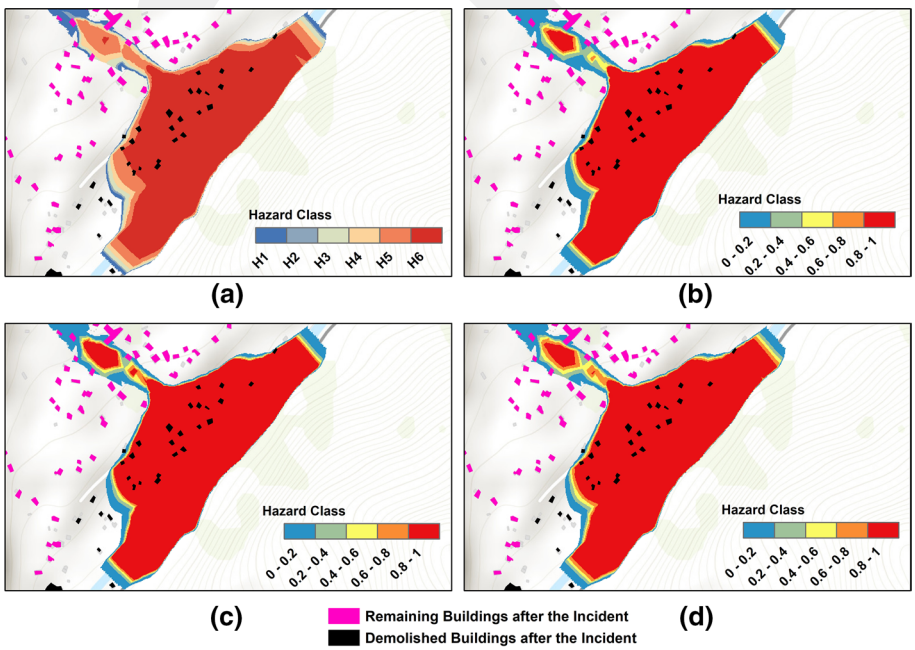

Fig. 19 Comparison of different hazard assessments **a** Smith et al. (2014), **b** Fuchs et al. (2007), **c** Akbas et al. 2009) and **d** Papathoma-Köhle et al. (2012)

risk assessment. There are minor differences at the just upstream of the inundation area. Hazard classes of H4, H5 and H6 are observed according to Newtonian hazard assessment method, whereas all risk levels are seen for non-Newtonian risk assessments. Besides, regardless of the hazard or risk assessment method, higher risk classes that can cause structural failure are observed where debris flow of 2015 incident demolished the buildings. Therefore, for the case investigated in the present study, it can be inferred that the preferred hazard assessment method does not change the results considerably. Moreover, buildings are digitized by considering satellite images before and after the incident and demolished buildings are determined. The main concern of this effort is to determine whether the demolished buildings are located within the high level of hazard zone. The results indicate that the red area of each hazard assessment methods covers the demolished buildings. Therefore, it can also be concluded from the demolished building images that each of the hazard assessment method (including Newtonian one) is eligible for debris hazard assessment although the debris hazard assessment methods have flow depth limitation.

5.4 Slope analysis

Debris flow occurs due to excess precipitation and rapid melting of snow (Decaulne et al. 2005). Moreover, if the slope is steeper, the downstream area is prone to excessive hazard. For this reason, slope analysis of the catchment where the debris incident took place is assessed and shown in Fig. 20. The complex slope classes of USDA Soil Survey Manual (Soil Science Division Staff 2017) are considered due to the lack of regular surface within the catchment area. Spatially varied slope classes are determined

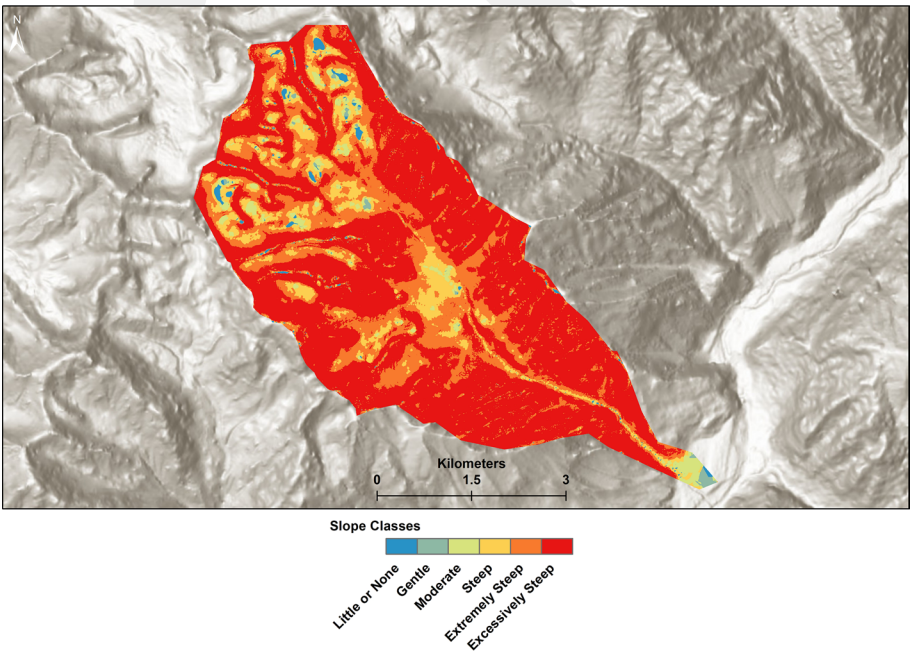

Fig. 20 Representation of slope gradient

by implementing GIS works. The slope is excessively steep close to the catchment boundaries, so that excessive precipitation would be conveyed through the edges of the catchment of Barsemdera Creek with mud and debris. Little or none classes slopes are observed near Gunt River where the 2015 debris flow hits the buildings. Moreover, the change in the slope class, especially from excessively steep to flat causes flow regime to change that can end up with extremely high flow depth.

6 Conclusions

According to IPCC (2018), global temperature has been increasing and the world goes through an irreversible process that adverse effects cannot be prevented. The debris flow incident of Barsem took place due to the heavy precipitation and excess temperature because of global warming, thus debris flow incidents can occur more frequently in future. In this study, a methodology for simulating debris flow and corresponding hazards is presented by considering emerging risks in a case study and the following conclusions could be drawn.

1. The study revealed that the DEM resolution does not have a significant effect on the inundation area, at least for the investigated case. However, there are dramatic differences in debris flow depth affecting hazard assessment. Therefore, free-source DEMs should be used carefully, especially in hazard classification. It should be noted that the SRTM DEM with 30 m resolution gives better predictions than the ALOS DEM of 12.5 m resolution. Consequently, while selecting the DEM source, the resolution should not be considered alone.
2. The flood hazard assessment suggested by Smith et al. (2014) and debris flow risk assessment suggested by Fuchs et al. (2007), Akbas et al. (2009) and Papathoma-Köhle et al. (2012) are considered in the present study. Although assessment of Newtonian flood hazard (Smith et al. 2014) considers the depth and the velocity, the exerted force caused by fluid would be much higher in case of debris flow. However, the results of the study show that Newtonian hazard assessment provide accurate predictions if the demolished structures are considered in the 2015 debris flow incident. Therefore, Newtonian hazard assessment proposed by Smith et al. (2014) may be a good candidate to be applied to debris flow incidents to determine risky areas. Along with these, the debris flow risk assessment techniques that are considered in this study give similar results.
3. In the present study hydrograph is not generated from the proposed formulations for the glacier lake outburst flood, because the duration of the hydrograph is very small compared to the real case. Therefore, a hydrograph including 14 consequent debris flows occurred during the 2015 debris flow incident is generated considering the field observations and previous reports (Fuchs 2015; REACT 2015). Although the duration of the used hydrograph is much higher than the duration calculated from the equations available in the literature, simulation results of the inundation area due to the generated hydrograph is very close to the real case. Consequently, it is safe to propose that in addition to the formulations for the hydrographs available in the literature, the unique situations of debris flow incidents should also be considered while deriving hydrographs.

Due to the changing precipitation regime and melting of glaciers, debris flow incidents may become more frequent, and the results of this study recommend an assessment for debris hazard so that decision makers can determine vulnerable areas.

Acknowledgements This study is a part of the Second Phase of the Central Asia Link Program—Sugd Oblast (CARs-2) and funded by World Bank. The authors take part in the project as researchers and are thankful to main contractor, Temelsu International Engineering Inc.

Data availability ALOS PALSAR: https://search.asf.alaska.edu/#/?zoom=5.915&center=96.406,16.491&dataset=ALOS, SRTM: https://www.usgs.gov/centers/eros/science/usgs-eros-archive-digital-elevation-shuttle-radar-topography-mission-srtm-1.

Declarations

Conflict of interest The authors reported no conflict of interest.

References

Akbas SO, Blahut J, Sterlacchini S (2009) Critical assessment of existing physical vulnerability estimation approaches for debris flows. Proc Landslide Process Geomorphol Mapp Dyn Model 1:229–233

ASTM (2017) Standard practice for classification of soils for engineering purposes (Unified Soil Classification System) D 2487–17

Braun A, Cuomo S, Petrosino S et al (2018) Numerical SPH analysis of debris flow run-out and related river damming scenarios for a local case study in SW China. Landslides 15:535–550. https://doi.org/10.1007/s10346-017-0885-9

Brunner GW (2021) HEC-RAS, River analysis system hydraulic reference manual. Davis, CA

Cannon SH, Gartner JE, Rupert MG, et al (2009) Emergency assessment of postfire debris-flow hazards for the 2009 station fire, San Gabriel Mountains, Southern California. Virginia. https://doi.org/10.3133/ofr20091227

Cesca M, D'Agostino V (2008) Comparison between FLO-2D and RAMMS in debris-flow modelling: a case study in the Dolomites. WIT Trans Eng Sci 60:197–206. https://doi.org/10.2495/DEB080201

Chidi CL, Zhao W, Chaudhary S et al (2021) Sensitivity assessment of spatial resolution difference in DEM for soil erosion estimation based on UAV observations: an experiment on agriculture terraces in the middle hill of Nepal. ISPRS Int J Geo-Inf 10(28):1–17. https://doi.org/10.3390/ijgi10010028

Cook SJ, Quincey DJ (2015) Estimating the volume of Alpine glacial lakes. Earth Surf Dyn 3:559–575. https://doi.org/10.5194/esurf-3-559-2015

Coussot P, Proust S (1996) Slow, unconfined spreading of a mudflow. J Geophys Res 101:217–229. https://doi.org/10.1029/96JB02486

Davies TRH (1990) Debris-flow surges-experimental simulation. J Hydrol: N Z 29:18–46

Decaulne A, Sæmundsson P, Pétursson O (2005) Debris flow triggered by rapid snowmelt: a case study in the Gleidarhjalli area, northwestern Iceland. Geogr Ann A Phys Geogr 87:487–500. https://doi.org/10.1111/j.0435-3676.2005.00273.x

Dokukin M, Chernomorets S, Savernyuk E, et al (2019) Barsem debris flow disaster in the Pamirs in 2015 and its analogues in the central Caucasus. Геориск XIII:26–36. https://doi.org/10.25296/1997-8669-2019-13-1-26-36

Floyd I, Sanchez A, Gibson S, Savant G (2020) A modular, non-Newtonian, model, library framework (Debris-Lib) for post-wildfire flood risk management. Hydrol Earth Syst Sci Discuss. https://doi.org/10.5194/hess-2020-509

Froehlich DC (1995) Peak outflow from breached embankment dam. J Water Resour Plan Manag 121:90–97. https://doi.org/10.1061/(ASCE)0733-9496(1995)121:1(90)

Fuchs S (2015) The Barsem disaster. Thun, Switzerland. https://www.ndr.ch/wp-content/uploads/2016/01/Barsem.pdf. Accessed 17 Mar 2022

Fuchs S, Heiss K, Hübl J (2007) Towards an empirical vulnerability function for use in debris flow risk assessment. Nat Hazards Earth Syst Sci 7:495–506. https://doi.org/10.5194/nhess-7-495-2007

Gibson S, Floyd I, Sánchez A, Heath R (2021) Comparing single-phase, non-Newtonian approaches with experimental results: validating flume-scale mud and debris flow in HEC-RAS. Earth Surf Process Landf 46:540–553. https://doi.org/10.1002/esp.5044

Gibson S, Sanchez A (2020) HEC-RAS mud and debris flow. Davis, CA

Gilany N, Iqbal J (2020) Geospatial analysis and simulation of glacial lake outburst flood hazard in Shyok Basin of Pakistan. Environ Earth Sci 79:1–11. https://doi.org/10.1007/s12665-020-8867-y

Guthrie R, Befus A (2021) DebrisFlow Predictor: an agent-based runout program for shallow landslides. Nat Hazards Earth Syst Sci 21:1029–1049. https://doi.org/10.5194/nhess-21-1029-2021
Hürlimann M, Copons R, Altimir J (2006) Detailed debris flow hazard assessment in Andorra: a multidisciplinary approach. Geomorphology 78:359–372. https://doi.org/10.1016/j.geomorph.2006.02.003
IPCC (2018) Global warming of 1.5°C. Special report, NYC: IPCC. Cambridge University Press. https://doi.org/10.1017/9781009157940
Jakob M, Hungr O (2005) Debris-flow hazards and related phenomena, 1st edn. Springer, Berlin
Kaitna R, Rickenmann D, Schatzmann M (2007) Experimental study on rheologic behaviour of debris flow material. Acta Geotech 2:71–85. https://doi.org/10.1007/s11440-007-0026-z
Kean JW, Staley DM, Lancaster JT et al (2019) Inundation, flow dynamics, and damage in the 9 January 2018 Montecito debris-flow event, California, USA: opportunities and challenges for post-wildfire risk assessment. Geosphere 15:1140–1163. https://doi.org/10.1130/GES02048.1
Mergili M, Fischer JT, Krenn J, Pudasaini SP (2017) R.avaflow v1, an advanced open-source computational framework for the propagation and interaction of two-phase mass flows. Geosci Model Dev 10:553–569. https://doi.org/10.5194/gmd-10-553-2017
O'Brien JS, Julien PY (1988) Laboratory analysis of mudflow properties. J Hydraul Eng 114:877–887. https://doi.org/10.1061/(ASCE)0733-9429(1988)114:8(877)
Papathoma-Köhle M, Keiler M, Totschnig R, Glade T (2012) Improvement of vulnerability curves using data from extreme events: debris flow event in South Tyrol. Nat Hazards 64:2083–2105. https://doi.org/10.1007/s11069-012-0105-9
Raetzo H, Lateltin O, Bollinger D, Tripet JP (2002) Hazard assessment in Switzerland—Codes of practice for mass movements. Bull Eng Geol Environ 61:263–268. https://doi.org/10.1007/s10064-002-0163-4
REACT (2015) Mudflow in Shughnan district, Gorno-Badakhshan Autonomous Oblast (GBAO). Tajikistan situation report # 2. https://reliefweb.int/report/tajikistan/mudflow-shughnan-district-gorno-badakhshan-autonomous-oblast-gbao-tajikistan-0. Accessed 17 Mar 2022
Saidov M, Ischuk N (2018) Natural hazards in Tajikistan, OSCE Technical report, Dushanbe. https://doi.org/10.13140/RG.2.2.35623.19368
Smith GP, Davey EK, Cox R (2014) Flood hazard. WRL Technical report 2014/07, University of New South Wales, Sydney. https://knowledge.aidr.org.au/media/2334/wrl-flood-hazard-techinical-report-september-2014.pdf. Accessed 07 Mar 2022
Soil Science Division Staff (2017) Soil survey manual. In Ditzler C, Scheffe K, Monger HC (eds), USDA Handbook 18. Government Printing Office, Washington, D.C
Tayebi SAM, Tayyebi SM, Pastor M (2021) Depth-integrated two-phase modeling of two real cases: a comparison between r.avaflow and GeoFlow-SPH codes. Appl Sci 11:1–19. https://doi.org/10.3390/app11125751
USAID (2018) Climate risk profile: Central Asia. Fact sheet. https://www.climatelinks.org/sites/default/files/asset/document/2018-April-30_USAID_CadmusCISF_Climate-Risk-Profile-Central-Asia.pdf. Accessed 10 Mar 2022
Varnes DJ (1978) Slope movement types and processes. In: Schuster RL, Krizek RJ (eds), Transportation and Road Research Board, National Academy of Science, Washington D.C., pp 11–33
Wahl TL (2004) Uncertainty of predictions of embankment dam breach parameters. J Hydraul Eng 130:389–397. https://doi.org/10.1061/ASCE0733-94292004130:5389
Zhang J, Wang F (2019) Regional temperature response in central Asia to national committed emission reductions. Int J Environ Res Public Health 16:1–15. https://doi.org/10.3390/ijerph16152661
Zhang T, Wang W, Gao T, An B (2021) Simulation and assessment of future glacial lake outburst floods in the Poiqu river basin, central Himalayas. Water (Switzerland) 13:1–18. https://doi.org/10.3390/w13101376
Zhao W, You Y, Chen X et al (2020) Case study on debris-flow hazard mitigation at a world natural heritage site, Jiuzhaigou Valley, Western China. Geomat Nat Hazards Risk 11:1782–1804. https://doi.org/10.1080/19475705.2020.1810784
Zimmermann M, Haeberli W (1992) Climatic change and debris flow activity high-mountain areas. A case study in the Swiss Alps. Catena Suppl 22:59–72